

Evaluation of the accuracy of the free-energy-minimization method

R. Najafabadi* and D. J. Srolovitz

Department of Materials Science and Engineering, University of Michigan, Ann Arbor, Michigan 48019-2136

(Received 2 March 1995)

We have made a detailed comparison between three competing methods for determining the free energies of solids and their defects: the thermodynamic integration of Monte Carlo (TIMC) data, the quasiharmonic (QH) model, and the free-energy-minimization (FEM) method. The accuracy of these methods decreases from the TIMC to QH to FEM method, while the computational efficiency improves in that order. All three methods yield perfect crystal lattice parameters and free energies at finite temperatures which are in good agreement for three different Cu interatomic potentials [embedded atom method (EAM), Morse and Lennard-Jones]. The FEM error (relative to the TIMC) in the (001) surface free energy and in the vacancy formation energy were found to be much larger for the EAM potential than for the other two potentials. Part of the errors in the FEM determination of the free energies are associated with anharmonicities in the interatomic potentials, with the remainder attributed to decoupling of the atomic vibrations. The anharmonicity of the EAM potential was found to be unphysically large compared with experimental vacancy formation entropy determinations. Based upon these results, we show that the FEM method provides a reasonable compromise between accuracy and computational demands. However, the accuracy of this approach is sensitive to the choice of interatomic potential and the nature of the defect to which it is being applied. The accuracy of the FEM is best in high-symmetry environments (perfect crystal, high-symmetry defects, etc.) and when used to describe materials where the anharmonicity is not too large.

I. INTRODUCTION

All equilibrium thermodynamic information about a system may be extracted from the free energy and its variation with respect to physical conditions. Therefore, considerable effort has been expended in developing methods to determine the free energy. Several methods have been proposed to extract thermodynamic data from atomistic simulations (see e.g., [Refs. 1–11] and a review in Ref. 12). Many of these simulation approaches require substantial computational resources^{1–7,10} and, hence, have never been applied to determine the free energies of complex systems, such as alloys, where significant composition fluctuations occur (e.g., due to surface segregation). Within the past six years, computationally efficient, approximate methods for extracting thermodynamic data from atomistic simulations have been developed.^{8,9,11} In the present paper, we examine the accuracy of these approximate methods and delineate the situations under which reasonably accurate results can be obtained.

The main idea behind these efficient methods^{8,9,11} is to determine the equilibrium atomic structure of the system by minimizing a free-energy functional with respect to the positions of all of the atoms. Hence, these methods are known collectively as the free-energy-minimization (FEM) method. In practice, the free-energy function is based upon a local version of the quasiharmonic method, where coupling between the individual atoms is ignored. For pure system, this approach reduces to the determination of one of the invariants of the N (3×3) dynamical matrices (one approach uses the trace, while another uses

the determinant—see below) associated with the N atoms in the system and hence the computational time scales linearly with the number of atoms in the system. The only input required to determine the free energy of any solid, atomic system are the atomic positions and an interatomic potential. A detailed description of the FEM method is presented in the next section.

In order to determine the accuracy of the FEM method, we compare the FEM results with results obtained from both more accurate quasiharmonic (QH) calculations and the thermodynamic integration technique as applied to Monte Carlo simulations (TIMC). The QH method has the advantage that it incorporates all of the coupling between the atoms within the system. As a result, this method requires the calculation of the determinant of the dynamical matrix of the entire system—typically an N^3 operation. Nonetheless, the QH method is still based on a harmonic picture of the solid, albeit at a lattice parameter which is adjusted to account for thermal expansion in a manner consistent with the interatomic potential. Monte Carlo simulations include all the anharmonicity of the interatomic potential as well as the coupling between all of the atoms. The free energy may be extracted from the Monte Carlo simulations by performing a series of simulations at different temperatures in order to determine the enthalpy $H(T)$ and then integrating $H(T)/T^2$ up to the temperature of interest. The accuracy of this approach is only limited by the statistics required to obtain $H(T)$. Very long MC simulations are required to obtain defect free energies with this method since the difference in $H(T)$ between a system with and without a defect (e.g., a vacancy) can be very small compared with the total enthalpy of the entire sys-

tem. This is what limits the computational efficiency of the determination of free energies from Monte Carlo simulations. Other MC methods, such as the overlapping distribution method, are of limited use in determining the free energy of defects at high temperature because of the inherent difficulty of handling defect migration and thermal generation of defects.¹³

One of the earliest applications of the free-energy-minimization method⁹ provided a careful comparison of the free energies of a perfect crystal and a vacancy using the FEM method and Monte Carlo simulations. These simulations were performed using a simple pair (Morse) potential and examined temperatures up to 75% of the melting point T_m . These comparisons showed agreement between the two approaches to calculating the perfect crystal free energy to within approximately 0.2% and within 2.5% for the vacancy formation free energy. Additional calculations were performed which compared FEM and QH results for the vacancy formation free energy for six metals¹⁴ using embedded atom method (EAM) potentials^{15–17} which showed agreement to within 6% in all cases. More recently, Foiles¹³ compared the free energies of defects (vacancy, grain boundary, and surface) using the FEM, QH, and Monte Carlo approaches and an EAM potential. He found that while good agreement was obtained for the perfect crystal free energy, poor agreement was found for the formation free energy of defects, with the vacancies exhibiting the largest discrepancy (as large as 65% at 1200 K in Cu). The large differences between the measured accuracies of the FEM compared with Monte Carlo data obtained with a simple pair potential and an EAM potential suggest that the accuracy depends on the type of interatomic potential employed. Furthermore, the good agreement between the QH and FEM calculations of the vacancy formation free energy and the poor agreement between the FEM and MC data on the same quantity indicate that a large part of the error is associated with the anharmonicity of the interatomic potential. Comparison of MC and FEM results on the formation energies of perfect crystals, surfaces, and grain boundaries consistently showed much smaller errors. In the present paper, we try to identify the properties of the interatomic potential that affect the accuracy of the FEM method, as well as delineate the types of defects where the FEM method can be expected to yield reliable results.

The outline of this paper is as follows. First, we describe the free-energy-minimization method, briefly outline the method for determining the free energy from Monte Carlo data, and discuss the interatomic potentials which are employed in the simulations. Next, the free energies of a perfect fcc crystal, an (001) surface, and a vacancy are presented based upon simulations performed with EAM potentials and two pair potentials—Morse and Lennard-Jones. In each case, we compare the results obtained using the TIMC, QH, and FEM approaches. Finally, we demonstrate the additional approximations used for studying alloy systems yield only very small errors in the free energy and that excellent agreement is obtained between MC and FEM calculations of the heat of segregation.

II. SIMULATION METHODOLOGY

A. Harmonic methods

The quasiharmonic approximation to the free energy of a perfect crystal¹⁸ has been shown to be very accurate up to temperatures in the vicinity of the melting point (based upon comparison with Monte Carlo results). Within the framework of this model, the Helmholtz free energy A_0 may be written as

$$A_0 = U + kT \int_0^\infty N(\omega) \ln \left[2 \sinh \left[\frac{\hbar\omega}{2kT} \right] \right] d\omega, \quad (1)$$

where U is the total potential energy determined by summing the interatomic potential over all atoms in the system, \hbar is Planck's constant, ω is the vibrational frequency, kT is the thermal energy, and $N(\omega)$ is the vibrational density of states. In the QH model, the vibrational density of states is determined from the $3N \times 3N$ dynamical matrix D ,

$$D_{i\alpha j\beta} = \frac{\partial^2 U}{\partial r_{i\alpha} \partial r_{j\beta}}, \quad (2)$$

where the subscripts i and j label atoms (1- N) and the subscripts α and β label directions (1-3). Since the number of atoms is finite, Eq. (1) can be rewritten as

$$A_0 = U + kT \sum_{i=1}^N \sum_{\beta=1}^3 \ln \left[2 \sinh \left[\frac{\hbar\omega_{i\beta}}{2kT} \right] \right], \quad (3)$$

where $\omega_{i\beta}$ are the $3N$ eigenvalues obtained from the diagonalization of the dynamical matrix D .

In the local harmonic (LH) model,⁹ we neglect all terms in the dynamical matrix that couple vibrations of different atoms. This approximation essentially decomposes the full $3N \times 3N$ dynamical matrix into N 3×3 local dynamical matrices. Diagonalization of these matrices yields $3N$ local vibrational frequencies, $\omega_{i\beta}$, which can be used in Eq. (3) to determine the local harmonic approximation to the free energy. In the LH model, the determinants of the local dynamical matrices are used to determine the free energy. In Sutton's second-moment model,^{8,11} the traces of the local dynamical matrices are employed.

In the classical approximation ($\hbar\omega \gg kT$), Eq. (3) reduces to

$$\begin{aligned} A_0 &= U + 3kT \ln \left[\left(\frac{\hbar}{kT\sqrt{M}} \right)^{N-1} |D|^{1/6} \right] \\ &\approx U + 3kT \sum_{i=1}^N \ln \left[\frac{\hbar |D_i|^{1/6}}{kT\sqrt{M}} \right] \\ &\approx U + 3kT \sum_{i=1}^N \ln \left[\frac{\hbar}{2kT} \left(\frac{2\text{Tr}(D_i)}{M} \right)^{1/2} + \frac{1}{4} \right], \end{aligned} \quad (4)$$

where M is the atomic mass and $|D|$ is the determinant of the dynamical matrix. The first expression in Eq. (4) applies to the QH model, where D is the full

$3(N-1) \times 3(N-1)$ dynamical matrix (where three rows and three columns have been deleted from the $3N \times 3N$ dynamical matrix to remove the translational degrees of freedom of the entire system). The second expression in Eq. (4) applies to the local harmonic method where $|D_i| = M^3[\omega_{i1}\omega_{i2}\omega_{i3}]^2$ is the determinant of the local dynamical matrix of atom i , and $|D_i|^{1/6}$ is the geometric average of the vibrational frequencies of atom i . The last expression in Eq. (4) represents the free energy in the second-moment approximation,^{8,11} where $\text{Tr}(D_i)$ is the trace of the local dynamical matrix.

Within the framework of the free-energy-minimization method, we obtain the finite temperature equilibrium structure by minimizing the free energy Eq. (4) with respect to the position of all of the atoms. This may be accomplished using a variety of techniques. In the calculation presented below, we have employed a conjugate gradient technique. The gradients of the free energy with respect to atomic displacements are finite temperature pseudoforces (i.e., the thermally averaged force), which are

$$f_{i\beta} = -\frac{\partial A_0}{\partial r_{i\beta}} = -\frac{\partial U}{\partial r_{i\beta}} - \frac{kT}{2} \sum_{j=1}^N \frac{1}{|D_j|} \frac{\partial |D_j|}{\partial r_{i\beta}}. \quad (5)$$

For a perfect cubic crystal, the free-energy minimization is reduced to a minimization with respect to one variable, the lattice constant a .

In order to study alloys, it is useful to introduce the concept of an "effective atom."¹⁹ Consider first the case of a binary alloy consisting of **a** and **b** atoms. If we were to monitor a particular atom site in such an alloy for a long time, we would find that that atomic site would be occupied by **a** atoms with probability c_a and by **b** atoms with probability $c_b = 1 - c_a$ (neglecting vacancies). Ignoring the temporal correlation between the site occupancies, we can then define the spatial compositional profile within the alloy crystal as $c_a(\mathbf{r})$. Within this framework, the vibrational free energy of the crystal may be described as in Eq. (4), with the atomic interactions used to describe the local dynamical matrix appropriately averaged (as described below) and the mass of the effective atom employed in the frequency calculations given by $m_i = c_a(i)m_a + c_b(i)m_b$.

In addition to the potential energy and the vibrational energy contributions to the free energy of an elemental solid described above, a description of the free energy of an alloy must also include the contribution associated with the configurational entropy. Several methods are available for determining the configuration entropy, including the Bragg-Williams approximation,²⁰ the cluster variation method,²¹ etc. The simplest approach to determine the configurational entropy is to use the Bragg-Williams approximation, which is a point approximation that ignores correlations. This is effectively the same level of approximation used to determine the vibrational contribution to the free energy within the local harmonic model. Therefore, we have adopted the Bragg-Williams approximation to determine the free energy within the free-energy-minimization method.¹⁹ This results in a

simple point approximation for the configurational entropy,

$$S_c = -k \sum_{i=1}^N \{c_a(i)\ln[c_a(i)] + c_b(i)\ln[c_b(i)]\}. \quad (6)$$

We note that since this expression always assumes no correlation between site occupancies, it is a rigorous upper bound to the true configurational entropy. In almost all situations, we note that at least some short-range correlation does exist. The assumption of no spatial correlations employed in obtaining Eq. (6) does not imply that spatial correlations will not form in our simulations, since spatial correlations predominantly are a result of the properties of the atomic interactions (except near critical points).

Within this "effective atom" approximation, the potential energy U is described as a sum over effective interatomic potentials. For example, the potential energy for pairwise interactions is simply

$$U = \sum_{i=1}^{N-1} \sum_{j=i+1}^N \{c_a(i)c_a(j)\phi_{aa}(r_{ij}) + [c_a(i)c_b(j) + c_b(i)c_a(j)]\phi_{ab}(r_{ij}) + c_b(i)c_b(j)\phi_{bb}(r_{ij})\}, \quad (7)$$

where $\phi_{aa}(r_{ij})$, $\phi_{ab}(r_{ij}) = \phi_{ba}(r_{ij})$, and $\phi_{bb}(r_{ij})$ are the pair potentials describing the energy of the bonds for *aa*, *ab*, and *bb* atom pairs, where the atoms are separated by a distance r_{ij} . The method used in obtaining the potential energy using EAM potential is very similar, as described in Ref. 19.

Defect free energies (e.g., grain boundary, surface, vacancy) are determined as the difference in free energy between a system containing the defect and one which is perfect, for the same number of atoms: $\Delta A = A_{\text{system}} - A_{\text{perfect}}$. Vacancy free energies were calculated by determining the free energies of a perfect crystal of 256 atoms and a crystal with one atom removed (i.e., one with a vacancy) and then subtracting: $\Delta A_{\text{vac}} = A_{255} - (\frac{255}{256})A_{256}$.

B. Thermodynamic integration of Monte Carlo data

The thermodynamic integration method is based upon the thermodynamic identity

$$\frac{d}{dT} \left[\frac{G}{T} \right] = -\frac{H}{T^2}, \quad (8)$$

where G and H are the free energy and enthalpy, respectively. The enthalpy is simply the average of the potential energy plus the average kinetic energy (assuming the pressure is zero—as in the present calculations). The average potential energy may be obtained as an ensemble average over many Monte Carlo steps, while the average kinetic energy is simply $3NkT/2$. Since the free energy of a defect is the difference between the free energies of the system with and without the defect (i.e., small differences of large numbers), long Monte Carlo runs are required in order to assure that sufficient statistical accu-

racy is obtained to guarantee the integrity of the defect free energies.

Equation (8) may be integrated to determine the free energy to within an unknown integration constant. This integration must be performed using $H(T)$ obtained at a constant pressure. In the results presented below, H was determined at 100 K increments ranging over 10^6 Monte Carlo steps per atom in a constant (zero) pressure Monte Carlo simulation. Equation (8) was integrated analytically using H which was fit to a third-order polynomial in T . The unknown integration constant resulting from the integration of Eq. (8) is arbitrarily chosen such that the MC and QH free energies match at 300 K.

C. Atomic interactions

Two classes of interatomic potentials were used in the present study in order to determine the sensitivity of the accuracy of the FEM method to the choice of interatomic potential. The two classes of potentials employed were central force pair potentials and embedded atom method potentials. Generic forms of pair potentials were chosen since they can easily be fit to any type of material and methods for scaling the results obtained with one set of parameters to others are well known. The first of these potentials employed is the common Lennard-Jones 6-12 potential which was cut off midway between the third and fourth nearest-neighbor separation in an fcc crystal and shifted up to zero energy at the cutoff [$\phi(r_c)=0$]. The two parameters σ and ϵ in the Lennard-Jones potential were determined by fitting to the equilibrium lattice parameter and sublimation energy of Cu ($\sigma=2.3276$ Å, $\epsilon=0.4912$ eV, and $r_c=5.4225$ Å). The second central force potential employed was the Morse potential $\phi(r)=D_0\{\exp[-2\alpha(r-r_0)]-\exp[-\alpha(r-r_0)]\}$. The three parameters in this potential were obtained by fitting to the equilibrium lattice parameter, sublimation energy, and bulk modulus of Cu and the potential was cut off midway between the third and fourth nearest-neighbor separation ($D_0=0.4262$ eV, $\alpha=1.3580$ Å⁻¹, $r_0=2.8110$ Å, and $r_c=5.4225$ Å). The Lennard-Jones and Morse potentials employed in the present study are shown in Fig. 1.

The second class of potential used in the present study was the embedded atom method form. Within the framework of the EAM, the total potential energy of the system is given by

$$U = \sum_{i=1}^{N-1} \sum_{j=i+1}^N \Phi(r_{ij}) + \sum_{i=1}^N F_i \left[\sum_{j \neq i} \rho_j(r_{ij}) \right], \quad (9)$$

where Φ_{ij} is the pair interaction between atoms i and j , $\rho_j(r_{ij})$ is the spherically averaged electron density of atom j at the position of atom i , and F_i is the energy required to embed atom i into the electron density due to all of its neighbors. The functions Φ , ρ , and F are determined by fitting empirical forms to experimental data (including the equilibrium lattice parameter, bulk modulus, sublimation energy, and vacancy formation energy) for Cu. $\Phi(r)$ and $\rho(r)$ were cut off between third and fourth nearest neighbors in an fcc crystal. Several forms of the

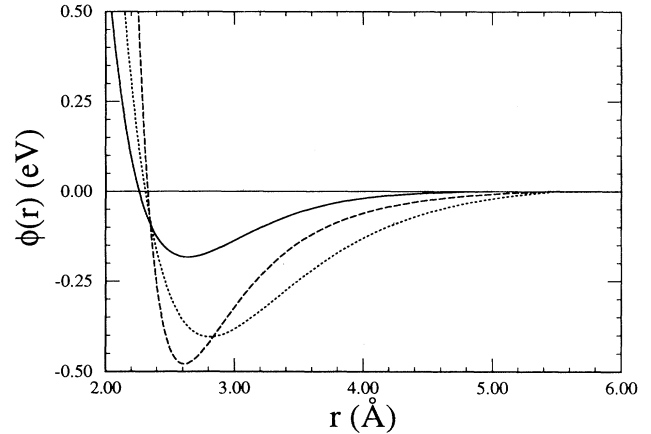


FIG. 1. The Cu interatomic potential $\phi(r)$ used in the present study. The dashed curve is the Lennard-Jones potential, the dotted curve is the Morse potential, and the solid curve is the effective EAM pair potential (obtained by expanding the many-body term about the zero temperature interatomic spacing, as described in the text).

EAM potentials for Cu are available. In the results presented below, we employed those of Ref. 17. However, we have obtained similar results using the Cu EAM potential of Ref. 16.

In order to compare the EAM potential with the Lennard-Jones and Morse potentials, we can write an effective EAM pair potential as $\phi(r)=\Phi(r)+2(dF/d\rho) \times (\rho-\rho_0)$, where ρ is the total electron density [i.e., the quantity in the square brackets in Eq. (9)], ρ_0 is ρ evaluated at the equilibrium, perfect crystal lattice parameter, and the derivative is evaluated at $\rho=\rho_0$. The effective EAM potential is plotted in Fig. 1. Note that although the EAM is much shallower than the other two potentials, all three potentials yield exactly the same cohesive energy (the effective EAM pair potential does not include a constant term from the embedding energy). The effective EAM potential is much more shallow and has a shorter repulsive region than either of the pair potentials. The shape of the EAM potential is much less symmetric about its minimum than either of the two pair potentials, while the Lennard-Jones potential is the most symmetric. By symmetric, we mean that the even terms in the expansion of the potential about its minimum dominate the odd terms.

III. PERFECT CRYSTAL RESULTS

All three interatomic potentials were used to determine the equilibrium face-centered-cubic lattice parameter a and zero pressure free energy G of a 256 atom simulation cell with periodic boundary conditions as a function of temperature in the FEM (local harmonic) and QH approximations and using the TIMC. The equilibrium lattice parameters as a function of temperature are shown in Fig. 2. Clearly the thermal expansions $\alpha=(da/dT)(1/a)$ predicted using all three methods are identical to within

10%. These errors translate into errors in the lattice parameter of less than 0.3% at the highest temperature examined (1200 K).

The temperature dependence of the zero pressure free energy G is shown in Fig. 3 for all three interatomic potentials and all three simulation methods. For each po-

tential, the entropy $S = -dG/dT$ is identical to within the statistical error in the Monte Carlo results. The errors in the enthalpy and hence the free energy (since the entropies are the same) are less than 1% for all three interatomic potentials at the highest temperature examined. We note, however, that there is some ambiguity in

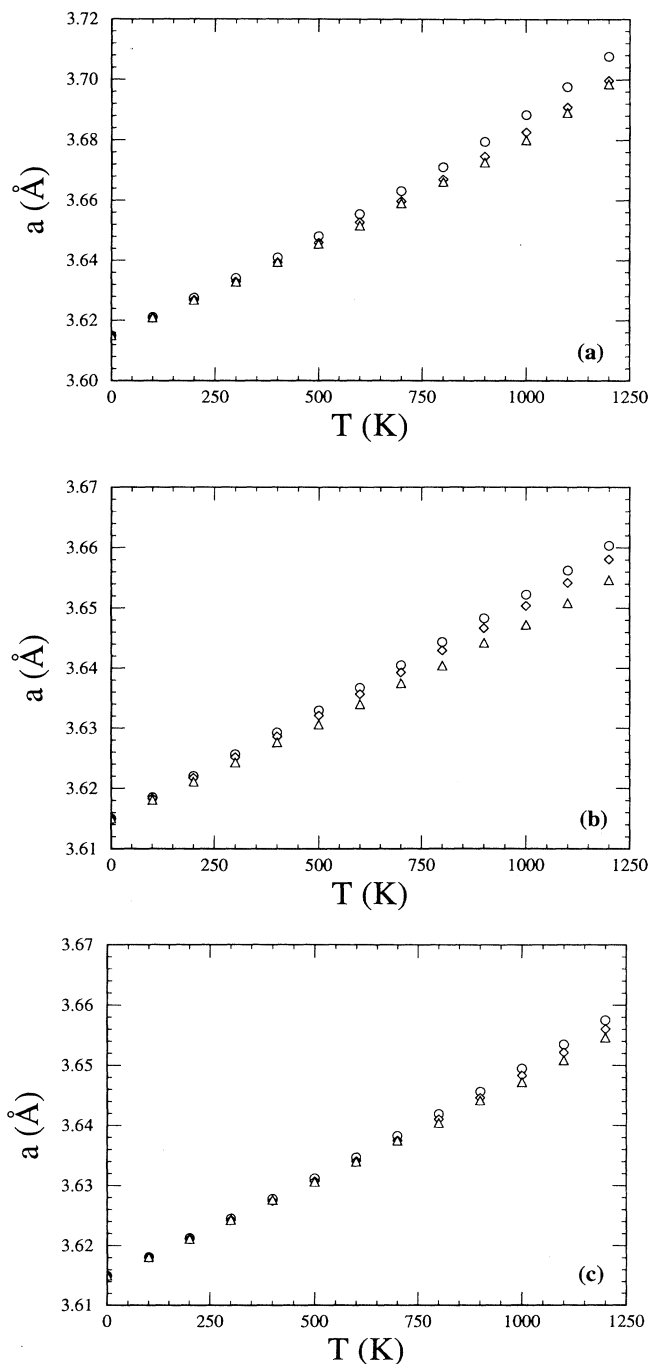


FIG. 2. The equilibrium face-centered-cubic lattice parameter a versus temperature T . The triangles represent FEM (local harmonic), the diamonds represent QH, and the circles represent TIMC calculations. (a), (b), and (c) are for simulations performed with the EAM, Morse, and Lennard-Jones potentials, respectively.

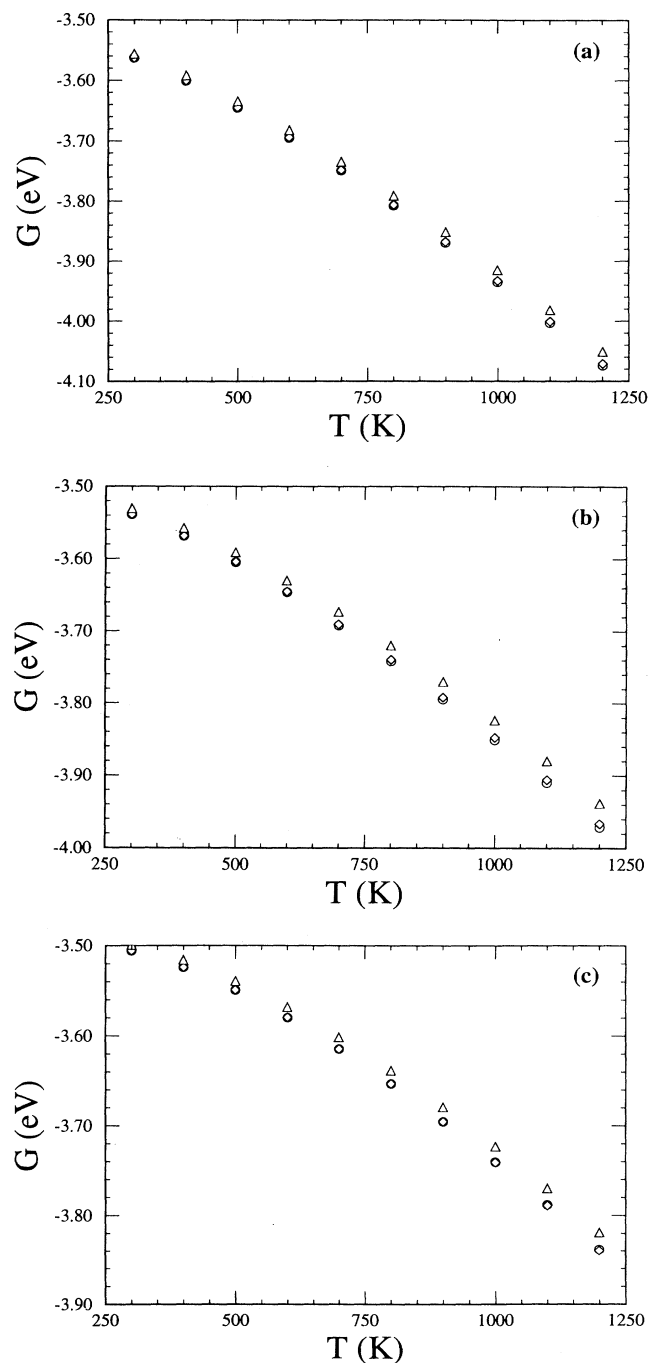


FIG. 3. The equilibrium perfect crystal free energy G versus temperature T . The triangles represent FEM (local harmonic), the diamonds represent QH, and the circles represent TIMC calculations. (a), (b), and (c) are for simulations performed with EAM, Morse, and Lennard-Jones potentials, respectively.

the free-energy results since the integration constant used to determine the free energy from the enthalpy was arbitrarily set equal to the QH value at 300 K.

The lattice parameter increases with increasing temperature, despite the fact that the FEM (local harmonic) and QH results are based upon the harmonic approximation. This clearly shows that all three simulation approaches do reasonably accurately account for the anharmonicity of the lattice, at least in a perfect crystal environment. These results also show that the FEM is a reliable method for predicting the thermodynamics of perfect crystals, while requiring only a small fraction of the computational resources required of the potentially (depending on the patience of the simulator) more accurate TIMC method. The present results for the EAM potentials are consistent with those found by Foiles¹³ to within statistical errors.

IV. (001) SURFACE RESULTS

The (001) surface of a face-centered-cubic crystal was simulated and the free energy determined as a function of temperature for all three interatomic potentials and all three methods for extracting the free energy. The size of the computational cell employed was $4a \times 4a$ in the plane of the surface and contained 16 (002) planes in the direction perpendicular to the surface. Periodic boundary conditions were employed in the directions parallel to the surface such that the in-plane lattice parameters were identical to that of an infinite bulk crystal at each temperature. The temperature dependence of the surface free energy γ_s is shown in Fig. 4 for all three potentials and all three methods of determining the free energy. There is a small discrepancy between the results presented in Fig. 4 for the EAM potential and those determined by Foiles,¹³ which is presumably attributable to statistical errors in the TIMC (see below).

There is increasing discrepancy between the (001) surface free energies calculated using the LH, QH, and TIMC methods as the temperature increases. This effect is clearly much more severe for the EAM potentials than for either the Morse or the Lennard-Jones potentials. The errors in the FEM surface free energies (relative to the MC data) are 1.7%, 3.9%, and 15% for the Lennard-Jones, Morse, and EAM potentials at 1200 K. This, however, is not an adequate test of the FEM method since most of the surface energy comes from the potential itself. A more critical appraisal of the FEM is with respect to the surface entropy $-d\gamma_s/dT$, for which the errors in the FEM analysis are 20%, 43.6%, and 75%. While the FEM results give the correct sign and order of magnitude of the surface entropy, the errors are, nonetheless, substantial.

The errors in the surface entropy may be traced to the fact that this quantity is sensitive to the anharmonicity of the potential and the lower symmetry of the surface environment with respect to the perfect crystal. As discussed below, the reason that the errors get progressively larger as we switch from Lennard-Jones to Morse to EAM potentials is that the anharmonicity of the EAM potential is larger than that for the Morse potential, which is larger

than that for the Lennard-Jones potential. The relatively large anharmonicity of the EAM potentials compared with the pair potentials is easily seen by considering the errors in the QH surface free energies. The difference between the QH and FEM free energies are associated with the neglect of the vibrational coupling between atoms.

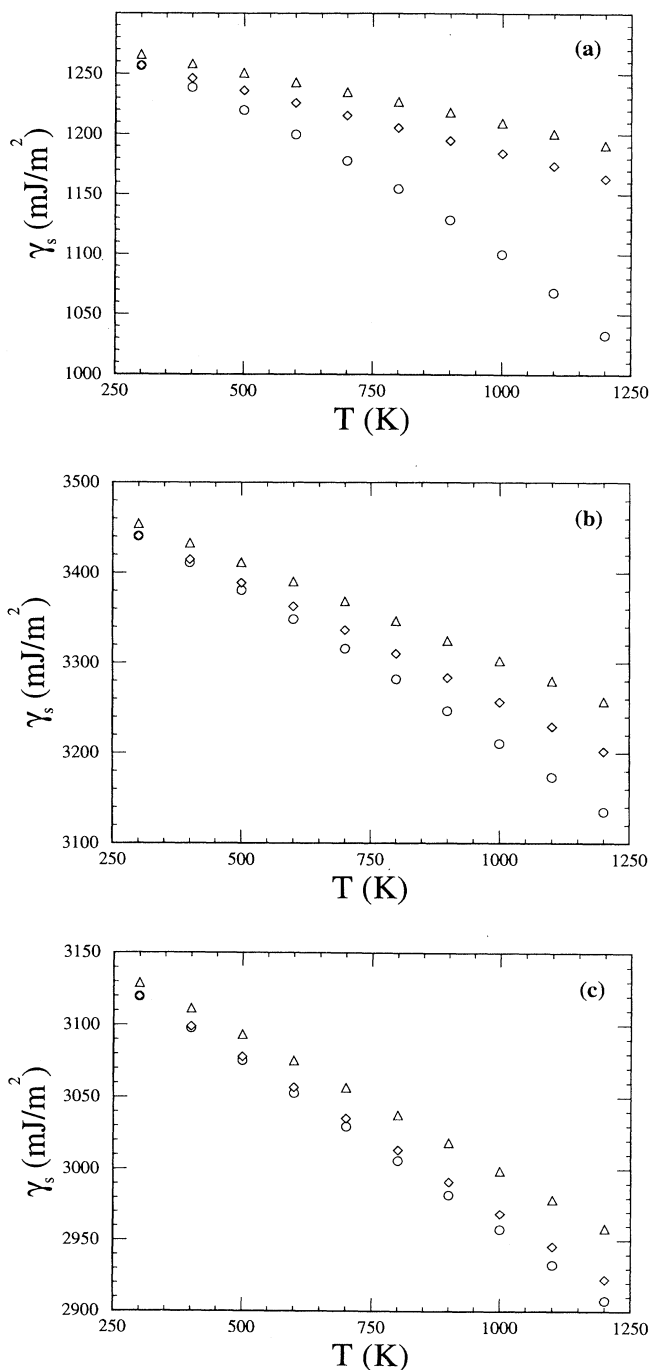


FIG. 4. The equilibrium (001) surface free energy γ_s versus temperature T . The triangles represent FEM (local harmonic), the diamonds represent QH, and the circles represent TIMC calculations. (a), (b), and (c) are for simulations performed with the EAM, Morse, and Lennard-Jones potentials, respectively.

On the other hand, the magnitude of the QH error itself (relative to the TIMC) is a measure of the anharmonicity of the atomic interactions. Examination of Fig. 4 demonstrates that the anharmonic contribution to the error completely dominates the errors obtained in the EAM case, while it is about equal to the vibrational coupling contribution in both of the pair potential cases.

In order to put the magnitude of the errors observed into proper perspective, we should consider the magnitude of the errors in the surface free energy with respect to experiment associated with the interatomic potentials and associated with the approximations to the vibrational contribution to the surface free energy. Unfortunately, no experimental free-energy data are available on the (001) surface of Cu; however, Wawra²² determined the polycrystalline average surface energy to be 2016 mJ/m². Fortunately, reliable first-principles (local-density approximation) calculations of the (001) surface energy of Cu (Ref. 23) are available and yield a value of 2300 mJ/m². The EAM potential, on the other hand, predicts an (001) surface energy of order 1200 mJ/m², which *underestimates* the true surface energy by 44%. Lennard-Jones and Morse potentials predict (001) surface energies of order 3100 mJ/m², which is an *overestimate* of 38% and 53%, respectively. Given the inaccuracies of the interatomic potentials for calculation surface energies of order $\pm 50\%$, the errors in the surface energies caused by the FEM method ($\leq 15\%$) are not very significant.

V. VACANCY RESULTS

The vacancy formation free energy was determined from MC and FEM simulations in which one atom was removed from the center of a 256 atom computational cell, with periodic boundary conditions set such that the bulk is of zero pressure. The statistical error in these MC calculations was large since the difference in enthalpies per particle in the system with and without a vacancy are small. Since the TIMC vacancy formation free energy g_{vac} is determined from the integration of the vacancy formation enthalpy h_{vac} , we show the enthalpy and the statistical error in the enthalpy as a function of temperature in Fig. 5. The TIMC error bars in Fig. 5 were deter-

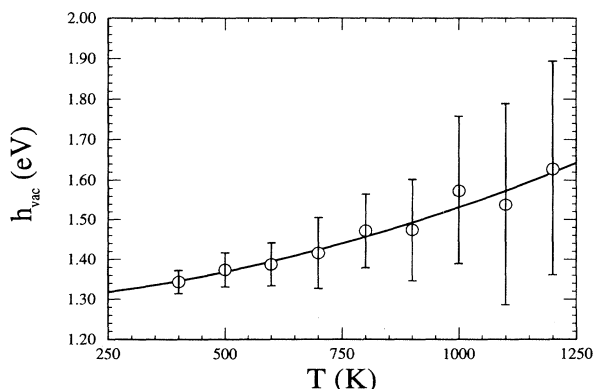


FIG. 5. The vacancy formation enthalpy h_{vac} vs T determined from Monte Carlo simulations using the EAM potential.

mined as follows: the first 10^5 Monte Carlo steps (MCS) per atom were used to equilibrate the system, the enthalpy data from the remaining 9×10^5 MCS were divided into nine bins of 10^5 MCS each, and the error bars were calculated as the standard deviation from the mean of these nine bins. For EAM, the statistical error is ± 0.27

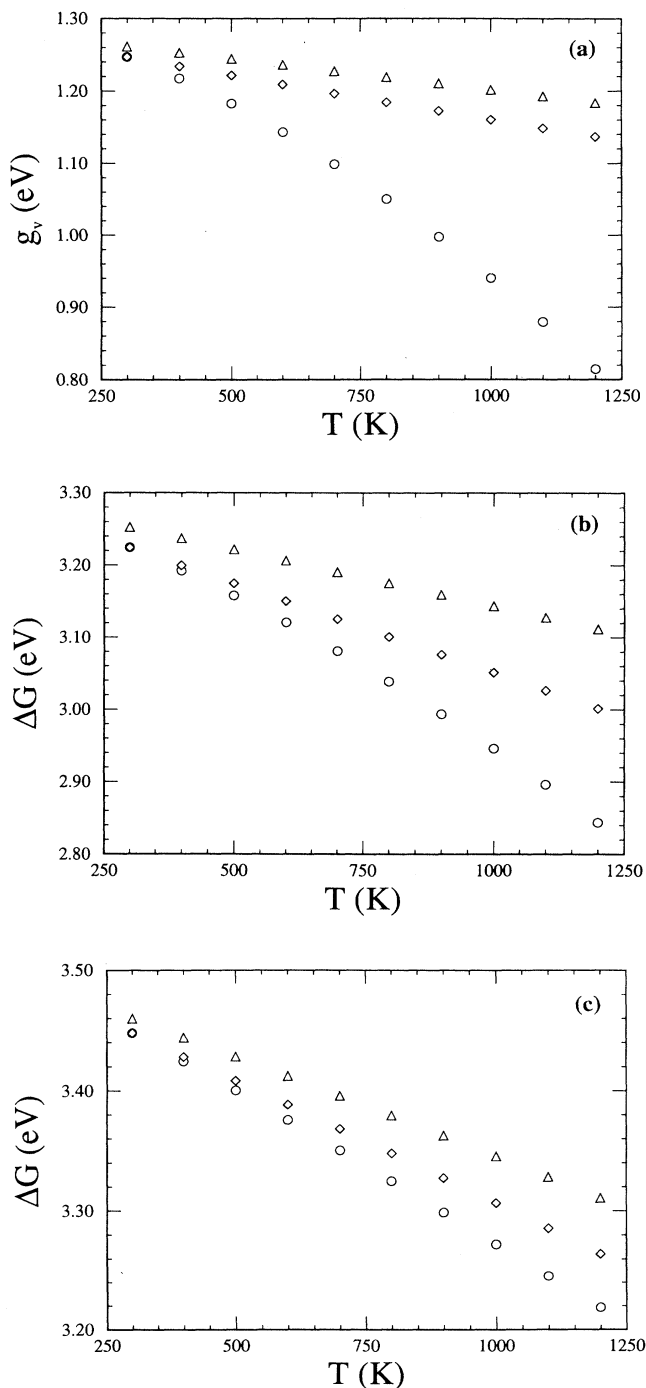


FIG. 6. The equilibrium (001) surface free energy g_{vac} versus temperature T . The triangles represent FEM (local harmonic), the diamonds represent QH, and the circles represent TIMC calculations. (a), (b), and (c) are for simulations performed with the EAM, Morse and Lennard-Jones potentials, respectively.

eV, which corresponds to a $\pm 17\%$ statistical error in the vacancy formation enthalpy at 1200 K. A similar calculation for the Lennard-Jones potential suggests a $\pm 3.4\%$ statistical error in the vacancy formation energy.

The temperature dependence of the vacancy formation free energy g_{vac} is shown in Fig. 6 for all three interatomic potentials and the three different methods used to obtain g_{vac} . Examination of Fig. 6 shows that the FEM errors in the vacancy formation free energy are largest for the EAM potential and smallest for the Lennard-Jones potential. Specifically, the errors in the FEM vacancy formation free energies at 1200 K are 35%, 9.5%, and 2.9% for the EAM, Morse, and Lennard-Jones potentials. Although the errors in the FEM vacancy formation energy are not too large for the pair potentials, the slopes dg_{vac}/dT show significantly greater errors: 86%, 70%, and 39% for EAM, Morse, and Lennard-Jones. The magnitudes of the vacancy formation energies are in much better agreement with experiment for the EAM potentials as compared with the pair potentials because the vacancy formation energy was used to determine the parameters in the EAM potentials.

In all case, the errors for the QH calculations for the vacancy formation energies are significantly less than for the FEM (local harmonic). Since the errors in the QH are approximately half that of the FEM when the pair potentials are used, we can attribute roughly half the FEM (local harmonic) error to the neglect of the vibrational coupling between atoms and the other half to anharmonicity effects. The difference between the QH and FEM errors in the vacancy formation free energy determined with the EAM potentials is similar to that found in the pair potential cases; however, the error attributable to anharmonicity (i.e., the QH error) is very much larger in the EAM case. This again points to the fact that the large anharmonicity of the EAM potentials is a major factor in determining the error in the FEM method.

$$E(y, x) = a_0 + \frac{1}{2}a_2(y+x)^2 + \frac{1}{2}a_3(y+x)^3 + \frac{1}{2}a_4(y+x)^4 + \frac{1}{2}a_2(y-x)^2 + \frac{1}{2}a_3(y-x)^3 + \frac{1}{2}a_4(y-x)^4 + \dots$$

$$= (a_0 + a_2y^2 + a_3y^3 + a_4y^4 + \dots) + (a_2 + 3a_3y + 6a_4y^2 + \dots)x^2 + (a_4 + \dots)x^4, \quad (11)$$

where terms in the expansion of the potential higher than fourth order have not been explicitly included. Note that because of the symmetry of the perfect crystal lattice, there are no terms in the energy that are odd in the displacement x . The vibrational contribution to the free energy may be determined with the local harmonic model by evaluating the energy at its finite temperature equilibrium lattice parameter $E(y, 0)$ and accounting for the vibrational contribution to the free energy as per Eq. (4). The vibrational frequency of an atom sitting in the potential well described by Eq. (11) and hence the free energy (within the harmonic approximation) may readily be determined using Eqs. (4) and (11) as

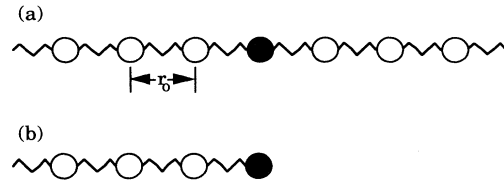


FIG. 7. Schematic illustration of the (a) one-dimensional perfect crystal and (b) a surface of that crystal.

VI. DISCUSSION

In order to separate the effects of symmetry, anharmonicity, and interatomic potential from the results of the free-energy-minimization method itself, it is useful to consider a few idealized situations. Consider first a one-dimensional crystal, where the atoms interact via a pair potential with a minimum at $r = r_0$, as shown in Fig. 7(a). We can expand the pair potential about its minimum as

$$\phi(r) = a_0 + a_2(r - r_0)^2 + a_3(r - r_0)^3 + a_4(r - r_0)^4 + \dots \quad (10)$$

In a perfect crystal environment with the potential cutoff between first and second nearest neighbors, the potential field around any individual atom is simply the sum of the contribution from its two nearest neighbors.

At a finite temperature, the lattice may expand, changing the lattice parameter by $y = r_0(T) - r_0(0)$, where $r_0(T)$ is the finite temperature lattice parameter. At finite temperature, each atom vibrates about its equilibrium lattice parameter $r_0(T)$ and hence, at any time, it may be displaced from y and x . Hence, the energy surface upon which an atom sits may be described by

$$A_0(y) = (a_0 + a_2y^2 + a_3y^3 + a_4y^4 + \dots)$$

$$+ kT \ln \left[\frac{\hbar}{kT\sqrt{M}} (4a_2 + 12a_3y + 24a_4y^2 + \dots) \right]. \quad (12)$$

The equilibrium lattice parameter is found by minimizing $A_0(y)$ with respect to y . Keeping terms to first order in y , the equilibrium lattice parameter is

$$r_0(T) = r_0(0) - \frac{3a_2a_3kT}{4a_2^3 + (12a_2a_4 + 9a_3^2)kT} \\ \approx r_0(0) - \frac{3a_3}{4a_2^2}kT + \frac{3a_3(12a_2a_4 - 9a_3^2)}{16a_2^5}(kT)^2, \quad (13)$$

where the second relation is found by expanding in T . The linear coefficient of thermal expansion is $-3a_3/(2a_2^2)$, where a_3 is typically negative. The free energy associated with the equilibrium lattice parameter is

$$A_0(T) = a_0 + \frac{kT}{2} \ln \left[\left(\frac{2\hbar}{kT} \right)^2 \frac{a_2}{M} \right] \\ - \left[\frac{9}{4} \right] \frac{a_3^2(kT)^2}{4a_2^3 + (12a_2a_4 - 9a_3^2)(kT)}. \quad (14)$$

Equations (12)–(14) demonstrate that all orders of

$$E(y, x) = \frac{1}{2}(a_0 + a_2y^2 + a_3y^3 + a_4y^4 + \dots) + \frac{1}{2}(2a_2y + 3a_3y^2 + 4a_4y^3 + \dots)x \\ + \frac{1}{2}(a_2 + 3a_3y + 6a_4y^2 + \dots)x^2 + \frac{1}{2}(a_3 + 4a_4y + \dots)x^3 + \frac{1}{2}(a_4 + \dots)x^4 + \dots \quad (15)$$

Comparing this energy surface with the one found for a perfect crystal [Eq. (11)], the most notable difference is that this energy surface contains terms with odd powers of the displacement x . The term that is linear in x would be zero if the energy were minimized with respect to the atomic coordinates such that each atom has zero force (i.e., $\partial E/\partial x = 0$). This would produce surface relaxation. However, even if the relaxation were performed (such that the linear term disappears), the other odd order terms (e.g., x^3) would remain. Therefore, the leading order correction term to the harmonic model in the defect case [Eq. (15)] scales as x^3 , instead of as x^4 as in the perfect crystal. The disappearance of the x^3 term in the perfect crystal is a result of the centrosymmetry of the perfect crystal environment. This shows that anharmonicity effects are more important (lower order) when the symmetry of the atomic environment is low.

The very good agreement between the MC and anharmonic (FEM and QH methods) results shown for the perfect crystal (see Sec. III) is attributable to the high symmetry of the atomic environment in the crystal. In this case, the anharmonic, cubic displacement terms (i.e., x^3) do not contribute to the errors in the harmonic free energies. The relatively poorer agreement between the MC and the harmonic results for the surfaces and vacancies is associated with the lower symmetry of the atomic environments in these cases. Hence, in these cases, the cubic terms in the displacement are responsible for the additional errors. Comparing the surface and vacancy free energy results, we found that significantly better agreement between the MC and the FEM methods occurred for the surfaces than for the vacancies. This too can be explained on the basis of the symmetry of the atomic environment. The (001) surface is centrosymmetric within the plane of the surface and is only asymmetric in the single direction, normal to the surface plane. In the vacancy

anharmonic terms (a_3, a_4, \dots) in the atomic interactions $\phi(r)$ are included in the harmonic description of the free energy. It is these anharmonic terms that lead to the thermal expansion of the lattice [Eq. (13)], despite the fact that the thermal expansion was determined within the harmonic approximation to the free energy. In a perfect crystal environment, the leading order correction to the anharmonic description of the energy in Eq. (11) scales as x^4 . The coefficient of the x^4 term depends on a_4 and higher order a_n but has no contribution from the leading order anharmonicity in the interatomic potential a_3 .

We now consider the case of a defect in a one-dimensional crystal. The simplest type of defect is made by cutting the infinite perfect crystal in two and removing one of the semi-infinite pieces [see Fig. 7(b)]. This creates a free surface. In this case, the atom at the end of the chain sees an energy surface of the form

case, on the other hand, the environment of an atom adjacent to the vacancy is not centrosymmetric in any direction. Therefore, the errors associated with the harmonic approximation become more severe as the symmetry of the local atomic environment becomes less. Foiles¹³ suggested that the lower symmetry of the atomic environment around defects (as compared with a perfect crystal) was the cause for the greater errors in the harmonic model in the defect case. The present analysis analytically shows the reason for this assertion. Although the simple model presented above is only one dimensional, group theoretical arguments can be made to show that the same types of effects of reducing symmetry around defects also hold in cubic crystals.

Examination of the results shown in Figs. 2–6 demonstrates that in all cases the errors in the FEM and QH results are always smaller for the Lennard-Jones and Morse potentials than for the EAM potential and that the errors for the Lennard-Jones potential are smaller than those for the Morse potential. As the above analysis shows, the error associated with the harmonic models is associated with the anharmonicity of the interatomic potential *not* included in the overall thermal expansion of the crystal. For defects, this error is dominated by the cubic terms in the displacement, the coefficient of which is related to the anharmonicity of the potential. Assuming that the goal of simulation studies is to correctly model real materials, it is important to evaluate how large these anharmonic terms are in real materials and to see how well the potentials represented them. Unfortunately, there are relatively little direct data available on the magnitude of these anharmonic terms. However, we can extract some useful information from experimental measurements of vacancy formation energies.

Since the errors in the harmonic models were larger for the EAM potential than for either of the two pair poten-

tials, we will focus on the EAM potential. The most reliable experimental vacancy formation data are obtained near the melting temperature T_m , where vacancy equilibration is fast. The melting temperatures of copper determined using the EAM and experiment are in good agreement (within approximately 20 K). There is some scatter in the experimental vacancy formation measurements²⁴ with the heat of formation h_{vac} of Cu in the range of 1.0–1.3 eV and the formation entropy s_{vac} in the range $1-3k$, where k is Boltzmann's constant. The best current estimates for the Cu vacancy formation data²⁵ are $h_{\text{vac}} = 1.19$ eV and $s_{\text{vac}} = 3k$. Our EAM Monte Carlo data yield $s_{\text{vac}} = 7.3k$. This difference in s_{vac} is very significant since it translates into an error of nearly a factor of 100 in the vacancy concentration (assuming h_{vac} is properly determined). The experimental error in the vacancy concentration near the melting point is typically no larger than 10%. The discrepancy between the simulation estimates and the experimental data on the vacancy formation entropy is even larger than these results suggest, since the experimental data includes (positive) configurational contributions to the entropy, while such contributions are absent in the simulations. A comparison of h_{vac} is not meaningful since the EAM potential was fit to those data. This large discrepancy between the vacancy formation entropy determined using the EAM potential and experiment shows that the EAM potential greatly exaggerates the true anharmonicity of the material. The fact that the EAM potentials yield reasonable thermal expansions yet erroneous defect energies is simply attributable to the fact that the thermal expansion is simply proportional to a_3 , while the defect free energies are also sensitive to higher order anharmonic terms.

Switching now to the Lennard-Jones potential, the MC data predict a vacancy entropy of $s_{\text{vac}} = 3.0k$ which is in excellent agreement with experiment.²⁵ Therefore, while the EAM potential is superior to the simple Lennard-Jones potential in many ways, the Lennard-Jones potential yields a superior estimate of the vacancy entropy and hence the anharmonicity. The ratios of the vacancy concentrations obtained with the harmonic and MC methods (assuming the same h_{vac} , i.e., $\exp[s_{\text{vac}}/k]$) are more than

two orders of magnitude larger when the EAM potential is used as compared to when the Lennard-Jones potential is used. Since the errors in the harmonic methods are so much larger when the EAM potential is used rather than the Lennard-Jones potential, we conclude that the errors are strongly potential dependent and are very large only when the potential has large anharmonicity. Because the EAM potentials yield rather poor agreement with the experimental s_{vac} , we also conclude that the EAM potential results are not particularly meaningful for such quantities as the vacancy formation entropy and the temperature dependence of finite temperature defect properties. This is unfortunate since we have used the EAM potentials to calculate finite temperature defect properties in several studies (e.g., Refs. 14,19,26–34). However, as the present vacancy formation entropy results demonstrate (Figs. 3, 4, 6), the errors in the FEM are in the opposite direction from those in the finite temperature behavior of the EAM and so there is some cancellation of errors.

We have performed several studies^{19,27–34} where we have used the FEM method to examine segregation to surfaces and grain boundaries in metals using EAM potentials. The large discrepancies found between the FEM and MC results using the EAM potentials above force us to question the validity of our earlier results. Rittner, Foiles, and Seidman³⁵ made a direct comparison of the FEM with MC data for surface segregation free energies. They examined the (111) surface segregation free energies of all combinations of solute and solvent possible using six different metals modeled with EAM potentials. Their results (their Table III) are reproduced in Table I, below. Overall, the agreement between the MC and FEM segregation free-energy data is excellent. Of the 30 solute-solvent pairs considered, only four have errors of greater than 0.03 eV, where the average value of the segregation free energy is approximately 0.21 eV. The only potential problem is in those few cases where the segregation free energy is very small and the error may result in a change in sign; however, this only occurs for two out of 30 cases (where the magnitude of the segregation energies is of order 0.03 eV). These data show that despite the inaccuracies in applying the FEM with EAM potentials demon-

TABLE I. Comparison of the FEM and MC methods for calculating the (111) surface segregation free energies at 1000 K using EAM potentials. These results are reproduced from Ref. 35. The values are in units of electron volts (eV).

Solute atom	Solvent atom					
	Cu	Ag	Au	Ni	Pd	Pt
Cu-FEM		-0.07	-0.02	0.10	-0.01	0.02
Cu-MC		-0.11	-0.14	0.10	-0.01	0.00
Ag-FEM	0.33		0.08	0.50	0.26	0.38
Ag-MC	0.33		0.08	0.50	0.26	0.37
Au-FEM	0.25	-0.11		0.59	0.17	0.40
Au-MC	0.24	-0.11		0.58	0.16	0.39
Ni-FEM	-0.06		-0.06		-0.04	0.02
Ni-MC	-0.06	-0.11	-0.13		0.01	-0.01
Pd-FEM	0.04	-0.21	-0.18	0.36		0.16
Pd-MC	0.04	-0.21	-0.18	0.36		0.15
Pt-FEM	-0.19	-0.33	-0.28	0.09	-0.15	
Pt-MC	-0.19	-0.33	-0.28	0.09	-0.15	

strated above, the FEM/EAM combination *does* yield accurate estimates of the segregation free energies, even at elevated temperatures where the errors should be worse. Another possible source of error in using the FEM method for segregation calculations is in the "effective atom" and Bragg-Williams approximations. However, as we show below in the only evaluations of these approximations for segregation performed to date, the effective atom and Bragg-Williams approximations lead to insignificant errors in segregation simulations.

The free energy of segregation is simply the difference in energy of the system between putting a solute atom in the bulk and at the surface, $\Delta A = \Delta A_{\text{surface}} - \Delta A_{\text{bulk}}$, where $\Delta A_{\text{surface}}$ and ΔA_{bulk} are the difference in free energy of the surface and bulk, respectively, with and without the solute. While the local harmonic model will certainly introduce errors into the calculations of the surface energies, those errors will largely cancel out when we calculate $\Delta A_{\text{surface}}$ as the difference between the free energy of the surface with and without the solute. A similar conclusion can be drawn for the bulk. These conclusions should be valid when the solute is not too much different in size from the solvent. This is supported by the results of Rittner, Foiles, and Seidman,³⁵ who showed that the FEM and MC predictions of the segregation energies are in excellent agreement except where the solvent atoms are much bigger than the solute atoms (this is also consistent with the finding that the FEM errors are larger for vacancies than other defects).

VII. CONCLUSIONS

We have made a detailed comparison between three competing methods for determining the free energies of solids and their defects. The most accurate method is the thermodynamic integration method applied to Monte Carlo data. In order to obtain adequate statistical accuracy for determination of defect thermodynamic properties, this method requires a very large number of Monte Carlo steps per atom and hence demands substantial computational resources. The quasiharmonic model is based upon the assumption that atoms vibrate within quadratic potential wells, which are determined from the interatomic potential and the crystal structure at the appropriate finite temperature lattice parameter. This method is very accurate as long as the anharmonicities in the interatomic potential are not too large. The computational time required to apply this method typically scales as the cube of the number of atoms, N . The least accurate approach is the free-energy-minimization method based upon the local harmonic (or closely related) approximations. This method is similar to the quasiharmonic approximation, except that the vibrations of the different atoms are assumed to be uncoupled. Application of this method requires computations that scale linearly with N .

In our applications of this method to determining the lattice parameter and free energy of a perfect, face-centered-cubic Cu crystal (as described by three different interatomic potentials), the predictions of the TIMC, QH, and FEM methods were all found to be in good

agreement. The (001) Cu surface free energies determined using the FEM method differed from the TIMC results by as much as 15% using the EAM potential at 1200 K. The FEM error (relative to the TIMC) in the vacancy formation energy was 35% using the EAM potential at 1200 K. Similar surface and vacancy calculations using Morse and Lennard-Jones potentials showed errors which were 75% to 90% smaller than with the EAM potentials. Approximately one-half of the errors in the FEM determination of the free energies is associated with anharmonicities in the interatomic potentials, with the remainder attributed to decoupling of the atomic vibrations. The large errors associated with defects in Cu described by the EAM potential were traced to the large anharmonicity in that potential. The anharmonicity of the EAM potential was found to be unphysically large compared with vacancy formation entropy determinations. While the Morse and Lennard-Jones are generally inferior to the EAM potential in determining zero temperature properties and the thermal expansion coefficients, they do yield better agreement with vacancy formation entropy experiments. Based upon these results, we conclude that the FEM method provides a reasonable compromise between accuracy and computational demands. However, the accuracy of this approach is sensitive to the choice of interatomic potential and the nature of the defect to which it is being applied. The accuracy of the FEM is best in high-symmetry environments (perfect crystal, high symmetry defects, etc.) and when used to describe materials where the anharmonicity is not too large. In applications to interfacial segregation, the other (nonvibrational) approximations in the FEM method are reasonably accurate. In most situations, the approximations inherent in the FEM method are less severe than those inherent in the empirical interatomic potentials themselves.

ACKNOWLEDGMENTS

The authors gratefully acknowledge useful discussions with Professor J. Rickman of Lehigh University and thank Dr. S. Foiles of Sandia National Laboratory and Professor D. Seidman of Northwestern University for providing us with preprints of their work. This work was supported by the Division of Materials Science of the U.S. Department of Energy (Grant No. FG02-88ER-45367).

APPENDIX: TEST OF BRAGG-WILLIAMS AND EFFECTIVE ATOM APPROXIMATIONS IN SEGREGATION

In a recent paper, Rittner, Foiles, and Seidman³⁵ examined the accuracy of the FEM method for studies of surface segregation by computing segregation free energies with the Monte Carlo method and the FEM method. Their results clearly demonstrated that the FEM method yielded reliable estimates of the segregation free energy by examining binary pairs of each of six elemental metals. In the very few cases where the discrepancy was appreciable, the absolute magnitude of the segregation free en-

ergy was very small. However, in those cases statistical accuracy issues suggest that the Monte Carlo data should be viewed with some caution (see above). Despite this overall good agreement, Rittner, Foiles, and Seidman³⁵ suggested that the FEM method may still not be sufficiently accurate because of the use of the effective atom and Bragg-Williams approximations. In the course of a separate study on surface segregation in metal oxides,³⁶ we have had occasion to isolate the effects of the Bragg-Williams and effective atom approximations from the other aspects of the FEM method. Although we find that the local harmonic approximation is not accurate for ionic crystals due to the long-range nature of the bonding, this system does provide an accurate test vehicle for the Bragg-Williams and effective atom approximations.

We determined the surface segregation profile (concentration as a function of distance from the surface) to the (001) and (011) surfaces of $(\text{Fe}_{0.12}\text{Mn}_{0.88})\text{O}$ and $(\text{Co}_{0.3}\text{Ni}_{0.7})\text{O}$ using both the Monte Carlo and FEM methods. The atomic interactions were described within the framework of the classical shell model.³⁷ In order to separate effects of the local harmonic approximation from those of the Bragg-Williams and effective atom approximations, we determined the relaxed surface structure using the FEM method without adjusting the concentration profile. Next, using these frozen atomic positions, we determined the segregation profile using both the Monte Carlo and the FEM methods at the same temperature (1000 K). The *worst* agreement was found for the (011) surface of $(\text{Fe}_{0.12}\text{Mn}_{0.88})\text{O}$, which is reproduced in Fig. 8. Mn was found to segregate to this surface with an oscillatory segregation profile that decayed with distance into the bulk. A comparison of the MC and FEM segregation profiles show that the two methods produce quantitatively indistinguishable results to within the statistical accuracy of the MC data. The oscillatory behavior continues deep into the bulk in the FEM data, although this behavior is not observed in the MC data beyond the fifth layer. We believe that beyond the fifth layer, the statistics from these 10^4 MC steps per particle simulations make the MC data unreliable to predict these fine features.

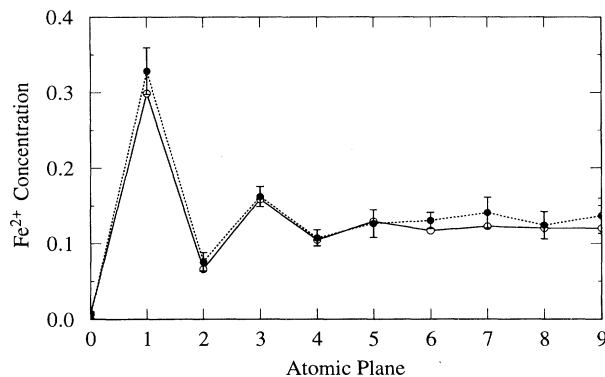


FIG. 8. The equilibrium (011) surface segregation profile in the mixed oxide $(\text{Fe}_{0.12}\text{Mn}_{0.88})\text{O}$ at 1,000 K. The solid curve and open symbols correspond to FEM calculations. The dashed curve and closed symbols represent Monte Carlo simulations performed using the atomic positions determined from the FEM calculations.

Although this study was performed on only two different surfaces of two different alloys, the excellent agreement between the MC and FEM results clearly show that the Bragg-Williams and effective atom approximations do not yield unreliable segregation data and, in fact, yield reliable (at least for these two cases) segregation data. Similar studies on segregation in metals are underway to determine the effect of these approximations. Rittner, Foiles, and Seidman³⁵ suggested that the errors in the Bragg-Williams approximation will lead to decreasing reliability for nondilute systems. This is clearly refuted by the present calculations where the Fe composition was 12%. Despite the success of the Bragg-Williams and the effective atom approximations in predicting segregation behavior, we do *not* expect that these approximations will lead to reliable predictions of certain other thermodynamic data, such as phase diagrams, especially in the vicinity of critical points.

*Present address: Knolls Atomic Power Laboratory, Schenectady, NY 12309.

¹B. Widom, *J. Chem. Phys.* **39**, 2808 (1963).

²I. R. McDonald and K. Singer, *Discuss. Faraday, Soc.* **43**, 40 (1967).

³I. R. McDonald and K. Singer, *J. Chem. Phys.* **47**, 4766 (1967); **50**, 2308 (1969).

⁴C. H. Bennet, *J. Comput. Phys.* **22**, 245 (1976).

⁵D. Frenkel and A. J. C. Ladd, *J. Chem. Phys.* **81**, 3188 (1984).

⁶G. M. Torrie and J. P. Valleau, *J. Comput. Phys.* **23**, 187 (1977).

⁷J. Q. Broughton and X. P. Li, *Phys. Rev. B* **35**, 9120 (1987).

⁸A. P. Sutton, *Philos. Mag. A* **60**, 147 (1989).

⁹R. LeSar, R. Najafabadi, and D. J. Srolovitz, *Phys. Rev. Lett.* **63**, 624 (1989).

¹⁰J. M. Rickman and S. R. Philpot, *J. Chem. Phys.* **95**, 7562 (1991).

¹¹A. P. Sutton, *Philos. Trans. R. Soc. London Ser. A* **341**, 233 (1992).

¹²D. Frenkel, in *Computer Simulation in Materials Science*, edited by M. Meyer and V. Pontikis (Kluwer, Dordrecht, 1991), p. 85.

¹³S. M. Foiles, *Phys. Rev. B* **49**, 14 930 (1994).

¹⁴L. Zhao, R. Najafabadi, and D. J. Srolovitz, *Modeling Simul. Mater. Sci. Eng.* **1**, 539 (1993).

¹⁵M. S. Daw and M. I. Baskes, *Phys. Rev. B* **29**, 6443 (1984).

¹⁶S. M. Foiles, *Phys. Rev. B* **32**, 7685 (1985).

¹⁷S. M. Foiles, M. I. Baskes, and M. S. Daw, *Phys. Rev. B* **33**, 7983 (1986).

¹⁸S. M. Foiles and G. B. Adams, *Phys. Rev. B* **40**, 5909 (1989).

- ¹⁹R. Najafabadi, H. Y. Wang, D. J. Srolovitz, and R. LeSar, *Acta Metall. Mater.* **39**, 3071 (1991).
- ²⁰W. L. Bragg and E. J. Williams, *Proc. R. Soc. A* **145**, 699 (1935); **151**, 50 (1935).
- ²¹R. Kikuchi, *Phys. Rev.* **81**, 988 (1951); J. M. Sanchez, F. Ducastelle, and D. Gratias, *Physica* **128A**, 334 (1984).
- ²²H. Wawra, *Z. Metallkd.* **66**, 395 (1975); **66**, 492 (1975).
- ²³J. G. Gay, J. R. Smith, R. Richter, F. J. Arlinghaus, and R. H. Wagoner, *J. Vac. Sci. Technol. A* **2**, 931 (1984); J. R. Smith, J. Ferrante, P. Vinet, J. G. Gay, R. Richter, and J. H. Rose, in *Chemistry and Physics of Fracture*, edited by R. H. Jones and R. M. Latanision (Martinus Nijhoff, Hingham, MA, 1987), p. 329.
- ²⁴A. N. Orlov and Yu. V. Trushin, *Energy of Point Defects in Metals* (Energoatomizdat, Moscow, 1983).
- ²⁵T. Hehenkamp, *J. Phys. Chem. Solids* **55**, 907 (1994).
- ²⁶L. Zhao, R. Najafabadi, and D. J. Srolovitz, *Philos. Mag. A* **70**, 519 (1994).
- ²⁷R. Najafabadi and D. J. Srolovitz, *Surf. Sci.* **286**, 104 (1993).
- ²⁸H. Y. Wang, R. Najafabadi, D. J. Srolovitz, and R. LeSar, *Acta Metall. Mater.* **41**, 2533 (1993).
- ²⁹H. Y. Wang, R. Najafabadi, D. J. Srolovitz, and R. LeSar, *Interface Sci.* **1**, 7 (1993).
- ³⁰H. Y. Wang, R. Najafabadi, D. J. Srolovitz, and R. LeSar, *Interface Sci.* **1**, 31 (1993).
- ³¹H. Y. Wang, R. Najafabadi, D. J. Srolovitz, and R. LeSar, *Phys. Rev.* **45**, 12 028 (1992).
- ³²H. Y. Wang, R. Najafabadi, D. J. Srolovitz, and R. LeSar, *Philos. Mag. A* **65**, 625 (1992).
- ³³H. Y. Wang, R. Najafabadi, D. J. Srolovitz, and R. LeSar, *Metall. Trans.* **23A**, 3105 (1992).
- ³⁴R. Najafabadi, H. Y. Wang, D. J. Srolovitz, and R. LeSar, *Scripta Metall. Mater.* **25**, 2497 (1991).
- ³⁵J. D. Rittner, S. M. Foiles, and D. N. Seidman, *Phys. Rev. B* **50**, 12 004 (1994).
- ³⁶C. Battaile, R. Najafabadi, and D. J. Srolovitz, in *Structure and Properties of Interfaces in Ceramics*, edited by D. Bonnel and M. Rühle, MRS Symposium Proceedings No. 357 (Materials Research Society, Pittsburgh, 1995).
- ³⁷B. G. Dick and A. W. Overhauser, *Phys. Rev.* **112**, 90 (1958).